J. Fluid Mech. (2009), *vol.* 630, *pp.* 367–390.
doi:10.1017/S0022112009006764 Printed in the United Kingdom

Oscillations of the large-scale circulation in turbulent Rayleigh–Bénard convection: the sloshing mode and its relationship with the torsional mode

QUAN ZHOU†, HENG-DONG XI, SHENG-QI ZHOU, CHAO SUN‡ AND KE-QING XIA¶

Department of Physics, The Chinese University of Hong Kong, Shatin, Hong Kong, China

(Received 7 August 2008 and in revised form 6 February 2009)

We report an experimental study of the large-scale circulation (LSC) in a turbulent Rayleigh–Bénard convection cell with aspect ratio unity. The temperature-extrema-extraction (TEE) method for obtaining the dynamic information of the LSC is presented. With this method, the azimuthal angular positions of the hot ascending and cold descending flows along the sidewall are identified from the measured instantaneous azimuthal temperature profile. The motion of the LSC is then decomposed into two different modes based on these two angles: the azimuthal mode and the translational or sloshing mode that is perpendicular to the vertical circulation plane of the LSC. Comparing to the previous sinusoidal-fitting (SF) method, it is found that both the TEE and the SF methods give the same information about the azimuthal motion of the LSC, but the TEE method in addition can provide information about the sloshing motion of the LSC. The sloshing motion is found to oscillate time-periodically around the cell's central vertical axis with an amplitude being nearly independent of the turbulent intensity and to have a $\pi/2$ phase difference with the torsional mode. It is further found that the azimuthal angular positions of the hot ascending and cold descending flows oscillate out of phase with each other by π, which leads to the observations of the torsional mode when these two flows are near the top and the bottom plates, respectively, and of the sloshing mode when they are both near the mid-height plane. A direct velocity measurement further confirms the existence of the bulk sloshing mode of the flow field.

1. Introduction

The phenomenon of thermal convection is ubiquitous in nature and in many engineering applications. A simple but paradigmatic model that has been widely used to study the convection phenomenon for more than a century is the turbulent Rayleigh–Bénard (RB) convection, which is a fluid layer heated from below and

† Present address: Shanghai Institute of Applied Mathematics and Mechanics, Shanghai University, Shanghai 200072, China.

‡ Present address: Physics of Fluids group, Faculty of Science and Technology, J. M. Burgers Centre for Fluid Dynamics, and Impact-Institute, University of Twente, 7500 AE Enschede, The Netherlands.

¶ Email address for correspondence: kxia@phy.cuhk.edu.hk

cooled on the top (for recent reviews, see Siggia 1994; Ahlers, Grossmann & Lohse in press). The dynamics of the RB system is determined by its geometry and two dimensionless control parameters: The Rayleigh number $Ra = \beta g H^3 \Delta T/\nu\kappa$ and the Prandtl number $Pr = \nu/\kappa$, where g is the gravitational acceleration, H the height of the cell, ΔT the temperature difference across the cell and β, ν and κ, respectively, the thermal expansion coefficient, the kinematic viscosity and the thermal diffusivity of the fluid. The geometry of the system is described by its symmetry and the aspect ratio of the convection cell Γ. For a cylindrical cell, $\Gamma = D/H$ with D being the cell's diameter.

A prominent feature of turbulent RB system is the presence of the large-scale circulation (LSC), which is self-organized from thermal plumes that erupt from the top and the bottom thermal boundary layers (Xi, Lam & Xia 2004). We call it 'large-scale' because it is a single cellular structure that spans the height of the cell, at least in cells with aspect ratios close to one. Since its discovery by Krishnamurti & Howard (1981) through flow visualization, the LSC, also called the mean wind, has been studied extensively using different techniques, such as flow visualization (Tilgner, Belmonte & Libchaber 1993; Funfschilling & Ahlers 2004; Xi *et al.* 2004), the laser Doppler technique (Qiu & Tong 2001*a*, *b*), ultrasonic technique in mercury (Mashiko *et al.* 2004), the particle image velocimetry (PIV) technique in water and in other high Prandtl number (Pr) fluids (Burr, Kinzelbach & Tsinober 2003; Xia, Sun & Zhou 2003; Xi *et al.* 2004; Sun, Xia & Tong 2005*b*; Xi, Zhou & Xia 2006), a floating flow-indicator method (Sun, Xi & Xia 2005*a*; Xi *et al.* 2006) and the multi-thermal-probe technique (Cioni, Ciliberto & Sommeria 1997; Brown, Nikolaenko & Ahlers 2005; Brown & Ahlers 2006; Sun & Xia 2007; Xi & Xia 2007, 2008*a*, *b*; Funfschilling, Brown & Ahlers 2008). The LSC is found to persist in fluids with extremely low values of Pr such as mercury (Cioni *et al.* 1997), moderate Pr such as helium gas (Niemela *et al.* 2001; Sreenivasan, Bershadskii & Niemela 2002) and water (Qiu & Tong 2001*a*, *b*) and other high Pr fluids (Xi *et al.* 2004). An intriguing feature of the LSC is that its motion can sometimes come to a complete halt momentarily and then restart in the same or different directions, these small-probability events are referred to as cessations and reversals. In an axial symmetric configuration, the LSC is also found to constantly undergoing stochastic azimuthal meandering and reorientations. These interesting dynamic features of the LSC will not be discussed in the present paper, and we refer interested readers to the recent review by Ahlers *et al.* (in press) and references therein.

Another intriguing feature of the LSC is that its motions near the top and the bottom plates of a cylindrical cell are found to exhibit a periodic azimuthal oscillation with a phase difference of π (Funfschilling & Ahlers 2004), which is referred to as the torsional mode of the LSC (Funfschilling *et al.* 2008). In addition to the torsional oscillation, there also exists a well-defined low-frequency oscillation in both the temperature and velocity fields, which has been long observed in turbulent RB experiments using various fluids (see, e.g. Castaing *et al.* 1989; Takeshita *et al.* 1996; Ashkenazi & Steinberg 1999; Qiu *et al.* 2000; Shang & Xia 2001; Qiu & Tong 2001*a*, 2002; Lam *et al.* 2002). Such oscillations are found not only in aspect-ratio-one cylindrical cells but also in larger-aspect-ratio cylindrical cells (Niemela & Sreenivasan 2006; du Puits, Resagk & Thess 2007) and in convection cells with other geometries, such as rectangular cells (Zhou, Sun & Xia 2007*b*). As oscillation is a common phenomenon in closed-flow systems, understanding the nature and the origin of the low-frequency oscillation in the RB system should be of general interest. To understand this oscillation, Villermaux (1995) proposed a mechanism of oscillations in the top and the bottom boundary layers of the system which are coupled by the LSC.

An implication of this model is that thermal plumes are emitted both periodically and alternately from the top and the bottom boundary layers. Some later experiments based on single-point or two-dimensional measurements of the temperature and velocity fields appear to support this picture (Ciliberto, Cioni & Laroche 1996; Qiu & Tong 2001*a*, 2002; Sun *et al.* 2005*b*; Tsuji *et al.* 2005). Some other works, however, pointed out that periodic plume emission is not necessary for the periodicity of the system (Funfschilling & Ahlers 2004; Resagk *et al.* 2006). Recently, Ahlers *et al.* (in press) conjectured that the low-frequency oscillation of the system presumably is due to the torsional oscillation of the LSC. However, the torsional mode alone is unable to explain the observed temperature and velocity oscillations at the mid-height plane of the cell, since simple twisting oscillations near the top and the bottom plates would cancel out at the mid-height plane because of symmetry.

In a recent experimental study of the three-dimensional spatial structure of the low-frequency temperature oscillations, Xi *et al.* (2009) showed that the low-frequency temperature oscillation at the cell's mid-height plane is due to the sloshing oscillation of the LSC. Their results showed convincingly and conclusively that the temperature oscillation in turbulent RB system is slaved to the oscillation of velocity field and thus temperature plays a passive role in the low-frequency oscillations; although the LSC itself is self-organized from thermal plumes (Xi *et al.* 2004) and driven by the buoyant forces of the plumes. It should be mentioned that a previous single-point velocity measurement has shown that at the cell centre the strongest velocity oscillation is along the direction perpendicular to the LSC plane and that the strength of this oscillation decays away from the cell centre towards the plates (Qiu *et al.* 2004). More recently, a study of the three-dimensional spatial structure of the velocity field has shown that the velocities along the axis perpendicular to the LSC plane and at the cell's mid-height plane correlate strongly with each other and have a common phase across the cell's entire diameter (Sun *et al.* 2005*b*). Both these results imply the existence of the sloshing mode of the LSC. However, the nature and the properties of this mode and its relationship with the torsional mode of the LSC have not been revealed, which are among the objectives of this paper.

The rest of the paper is organized as follows. We describe the experimental setup and conditions in § 2.1. In § 2.2, we describe in detail a method for extracting the azimuthal angular positions of the hottest and the coldest fluids along the sidewall and the LSC's central line from the measured instantaneous azimuthal temperature profile and provide a validation of this method. Comparisons with the previous sinusoidal-fitting (SF) method will also be made. The experimental results are presented and analysed in § 3, which is divided into three parts. In § 3.1 we present a detailed study of the sloshing oscillation of the LSC. Section 3.2 discusses the relationship between the sloshing mode and the torsional mode of the LSC and § 3.3 presents results from a direct velocity measurement of the bulk sloshing mode of the flow field. We summarize our findings and conclude in § 4.

2. Experimental setup, methods and parameters

2.1. *The convection cell and experimental conditions*

The experiment was carried out in a cylindrical cell with its top and bottom plates made of 1.5 cm thick copper, the sidewall of a 5 mm thick Plexiglas tube and water as convection fluid (Xi & Xia 2008*a*, *b*). The inner diameter D and the height H of the cell are both 19.0 cm and hence its aspect ratio Γ is unity. Twenty-four thermistors (Omega, 44031) with a diameter of 2.5 mm and an accuracy of 0.01° were

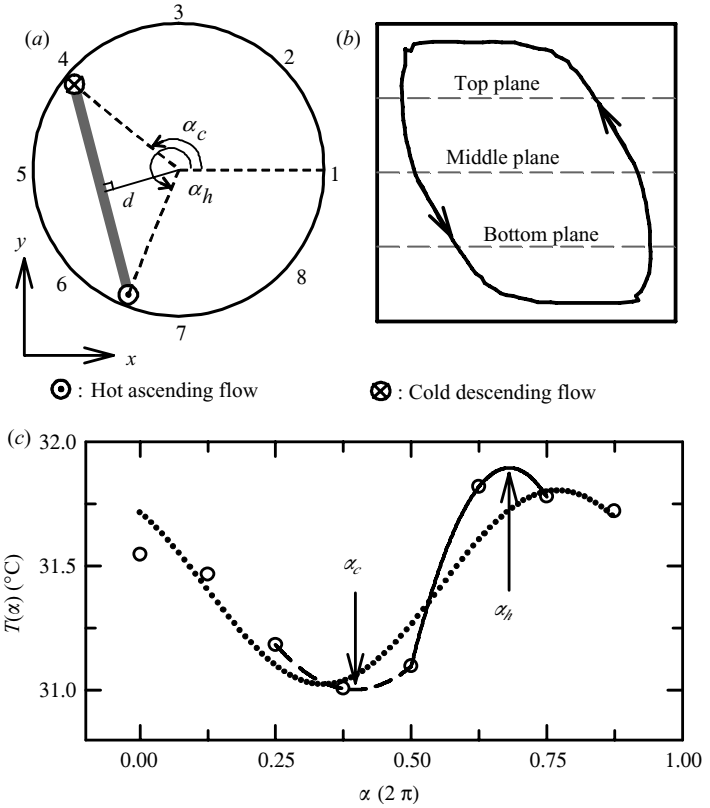

FIGURE 1. (*a*) Top-view of the convection cell and coordinate system used. Also shown is a typical instantaneous azimuthal positions α_h and α_c of the hot ascending and cold descending flows, corresponding to the temperature profile $T(\alpha)$ shown in (*c*). The *z*-axis (not shown in the figure) is along the cell's central vertical axis. The numbers 1–8 show the locations of the sidewall thermistors. (*b*) Side-view of the cell with measured circulation path of the LSC reproduced from Sun & Xia (2005). The three dashed lines show the top, middle and bottom planes where the thermistors are placed. (*c*) An example of a typical instantaneous temperature profile (open circles) measured by the eight thermistors at mid-height plane at $Ra = 5.5 \times 10^9$. The solid line represents a quadratic fit to the highest temperature reading and the two temperature readings adjacent to it. The dashed line represents a quadratic fit to the lowest temperature reading and the two temperature readings adjacent to it. The two vertical arrows indicate the fitted peak positions of α_h and α_c, respectively. The dotted line shows a sinusoidal fit to the profile. It is seen from the figure that, in this case, the sinusoidal fit to the profile shifts α_h to the right (anticlockwise in *a*) and shifts α_c to the left (clockwise in *a*).

placed in blind holes drilled horizontally from the outside into the sidewall with a distance of 0.7 mm from the fluid-contact surface. These thermistors are distributed in three horizontal rows at distances $H/4$, $H/2$ and $3H/4$ from the bottom plate, which are denoted as the bottom, middle and top planes (the three dashed lines in figure 1*b*), respectively, and in eight vertical columns equally spaced azimuthally around the cylinder (figure 1*a*). A multichannel multimetre was used to record the resistances of the 24 thermistors at a sampling rate of 0.29 Hz, which are converted into temperatures using calibration curves. Then the azimuthal temperature profile $T(\alpha)$ at the three heights can be obtained, where α is the azimuthal angle referenced to location 1. During the measurements, the mean temperature T_0 of the bulk fluid

was kept at 31°C and hence $Pr = 5.3$. The measurements covered six values of Ra, ranging from 9.0×10^8 to 6.0×10^9, and lasted 70–750 h.

In Xi *et al.* (2009) the cell was tilted by 2° to study the origin of the temperature oscillations. This is because in addition to the twisting and the sloshing motions, the orientation of the LSC also meanders randomly. By tilting the cell and thus locking the LSC orientation, one can remove the stochastic meandering from the signal and separate the complicated phenomena produced by the different types of motions. This enabled us to study the phase relationships between temperature oscillations at various locations. In this work, our focus is on the relationship between the twisting motion near the top and bottom plates and the sloshing motion at the mid-height plane. As the LSC meanders azimuthally as a whole across the height of the cell (Sun, Xi & Xia 2005*a*), the phase relationship between these two types of motions can be studied even with the azimuthal meandering present. Therefore, unless stated otherwise, all measurements in the present work were made with the cell levelled (to within $0 \pm 0.06°$).

As stated above, the temperature measurements in the present case are made with thermistors embedded in the sidewall, whereas in Xi *et al.* (2009) the sloshing motion was obtained from thermistors placed in fluid. It is known that the sidewall acts as a low-pass filter, thus the thermistors embedded in the sidewall are not sensitive to the high-frequency signals. Spatially, they actually sense the integrated signal over a finite area of the sidewall, which leads to a lowered strength of the detected sloshing oscillation as compared with that using the in-fluid probes. Nevertheless, as we will see below, the basic pictures obtained from the two cases are essentially the same. As one of the objectives of the present work is to understand the relationship between the sloshing oscillation and the twisting oscillations near the plates, we use data measured simultaneously by the 24 in-wall probes from the three heights (there are only eight in-fluid probes and that measurements can only be made at one height at a time). Thus, unless stated otherwise, all results presented in this paper were obtained from the in-wall probes.

2.2. *The temperature-extrema-extraction method*

An often-used method based on the multi-probe technique for extracting the dynamic information about the LSC motion is to fit the temperature azimuthal profile using a sinusoidal function, i.e. $T_k = T_a + A' \cos(k\pi/4 - \phi'),\ k = 0, 1, \ldots, 7$, where T_a is the azimuthal average of the eight temperature readings, A' is a measure of the strength of the LSC and ϕ' is the LSC's orientation (see, e.g. Cioni *et al.* 1997; Brown *et al.* 2005; Brown & Ahlers 2006; Xi & Xia 2007, 2008*a*, *b*; Funfschilling *et al.* 2008). This SF method has been very successful in the study of the azimuthal motion of the LSC, including rotations, cessations and reversals (see Ahlers *et al.* in press and references therein). However, the SF method requires the separation between the hottest and the coldest azimuthal positions to be π, i.e. the obtained LSC's central vertical plane (hereafter referred to as LSC's central line) is forced to always pass through the cell's central vertical axis, which, as we shall show below, is not always the case.

Here, we introduce the temperature-extrema-extraction (TEE) method that determines first the hottest and coldest azimuthal positions of the bulk fluid and then the central line of the LSC band. The TEE method has been described very briefly in Xi *et al.* (2009). In this section, we give its detailed description, validation and comparison with the SF method. To illustrate this method, figure 1(*c*) shows an example of the typical instantaneous temperature readings (circles) from the eight thermistors at mid-height plane. The hottest (coldest) azimuthal position of

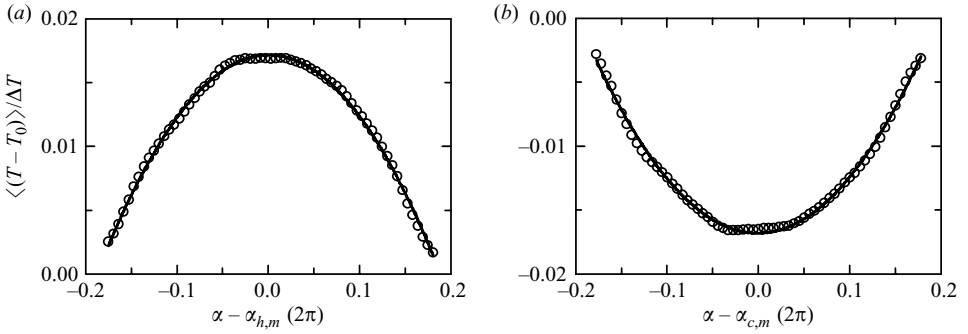

FIGURE 2. The averaged sidewall temperature profile $[T(\alpha)-T_0]$ normalized by the temperature difference ΔT around the fitted (a) hottest and (b) coldest azimuthal positions obtained at $Ra = 5.5 \times 10^9$. Solid lines are quadratic functions.

the bulk fluid along the sidewall was determined by making a quadratic fit around the highest (lowest) temperature reading. In practice, this requires only the local maximum (minimum) temperature and the two temperatures directly adjacent to it. This is because a quadratic function has three degrees-of-freedom and thus can be uniquely determined by only three data points. We label these azimuthal positions α_1, α_2 and α_3 with α_2 being the position of the local maximum (minimum) temperature. The position α_h (α_c) at any plane can then be found by solving analytically the three quadratic equations between $T(\alpha_k)$ and α_k ($k = 1, 2, 3$), i.e.

$$\alpha_h(\alpha_c) = \frac{1}{2}\frac{\left(\alpha_1^2-\alpha_2^2\right)[T(\alpha_2)-T(\alpha_3)]-\left(\alpha_2^2-\alpha_3^2\right)[T(\alpha_1)-T(\alpha_2)]}{(\alpha_1-\alpha_2)[T(\alpha_2)-T(\alpha_3)]-(\alpha_2-\alpha_3)[T(\alpha_1)-T(\alpha_2)]}. \tag{2.1}$$

In this paper, the subscripts 'h' and 'c' are used to denote the quantities associated with the hot ascending and cold descending flows, respectively, and the subscripts 't', 'm' and 'b' for the top, middle and bottom planes, respectively. Here we choose a quadratic function to fit the local temperature distribution because within a small range any temperature distribution, whether it is symmetric or not, can be expanded to a polynomial expression, which makes no physical assumption about the temperature distribution. As we have only three points around temperature extrema, a quadratic function is the best choice. To test the validity of the quadratic fit, figure 2 shows the normalized sidewall temperature profile. Each point is an average of $[T(\alpha_k)-T_0]/\Delta T$ ($k = \alpha_1, \alpha_2, \alpha_3$) in a bin with a small range around $\alpha - \alpha_{h,m}$ (figure 2a) or $\alpha - \alpha_{c,m}$ (figure 2b). The data around the hottest (figure 2a) and the coldest (figure 2b) positions are both in good agreement with the quadratic functions (solid lines), indicating that the quadratic function is indeed a good representation for the temperature distribution around the hot ascending and cold descending flows. With this method, the three rows of thermistors can thus provide simultaneously the azimuthal positions of the hot ascending and cold descending flows at the three heights, which are denoted as $\alpha_{h,t}$, $\alpha_{h,m}$ and $\alpha_{h,b}$, and $\alpha_{c,t}$, $\alpha_{c,m}$ and $\alpha_{c,b}$. With the obtained hottest and coldest positions, the line connecting the two positions is the central line of the LSC band. The orientation ϕ of this line is the orientation of the LSC, which is calculated as $\phi = (\alpha_c + \alpha_h + \pi)/2$ if $\alpha_c < \alpha_h$ and as $\phi = (\alpha_c + \alpha_h - \pi)/2$ if $\alpha_c > \alpha_h$, the distance between this line and the cell's central vertical axis is defined as the off-centre distance (see figure 1a) and $A = (T(\alpha_h) - T(\alpha_c))/2$ is used to characterize the strength of the LSC, where the factor $1/2$ is used in order to compare the obtained A with that obtained from the SF method. We denote ϕ_t, ϕ_m and ϕ_b, A_t, A_m and A_b and d_t, d_m

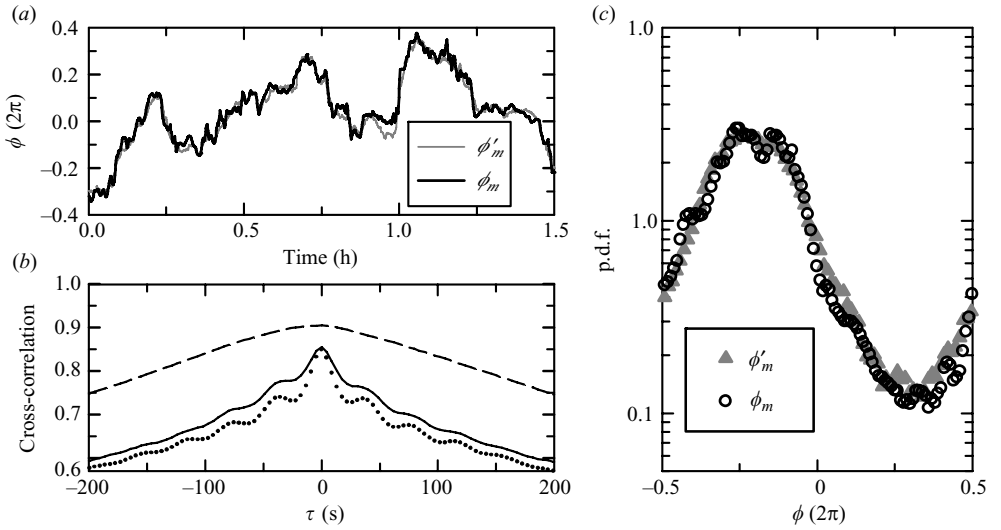

FIGURE 3. (*a*) Time traces of the orientation ϕ_m of the LSC central line obtained using the TEE method and the orientation ϕ'_m obtained from the SF method. (*b*) The cross-correlation functions between the orientations obtained using the two different methods for the top (solid line), middle (dashed line) and bottom (dotted line) planes. (*c*) p.d.f. of the two orientations ϕ_m and ϕ'_m. All data were measured at $Ra = 5.5 \times 10^9$.

and d_b as the orientations, the strengths and the off-centre distances of the LSC at the top middle, and bottom planes, respectively. Therefore, based on the TEE method, the motion of the LSC can be decomposed into two different modes: The azimuthal mode and the sloshing mode.

We now compare the orientations and the strengths of the LSC obtained using the TEE method and those obtained using the SF method. Figure 3(*a*) shows the time traces of ϕ_m and ϕ'_m, which are obtained using the same data set measured by the embedded thermistors. One sees that the time traces are very similar to each other. This similarity can be characterized by the coefficient of the cross-correlation between the two quantities. The cross-correlation function between two variables a and b is defined as

$$C_{a,b}(\tau) = \langle (a(t+\tau) - \langle a \rangle)(b(t) - \langle b \rangle) \rangle / \sigma_a \sigma_b, \tag{2.2}$$

where σ_a and σ_b are standard deviations of a and b, respectively, and $\langle \cdots \rangle$ represents the temporal average. When $a = b$, $C_{a,a}$, denoted as C_a, is the auto-correlation function of the variable a. Figure 3(*b*) shows the cross-correlation functions between ϕ and ϕ' at the three heights. It shows that all these three functions have a positive and strong correlation with the coefficient being all larger than 0.85 at time lag $\tau = 0$. (The subpeaks of C_{ϕ_t,ϕ'_t} and C_{ϕ_b,ϕ'_b} correspond to the twisting oscillations of the LSC near the top and the bottom plates.) It is further found that this strong positive correlation exists for all values of Ra investigated. Figure 3(*c*) shows the probability density functions (p.d.f.s) of ϕ_m and ϕ'_m. One sees that the two p.d.f.s essentially collapse on top of each other except that the distribution of ϕ'_m seems to be a little smoother than that of ϕ_m. This is due to the fact that ϕ_m is obtained from the azimuthal positions of the hot ascending and cold descending flows, which are determined by fitting a total of five to six thermistor readings, while ϕ'_m is from the global fitting to eight local temperatures. However, the basic pictures about the azimuthal motion of the LSC obtained from both methods are the same.

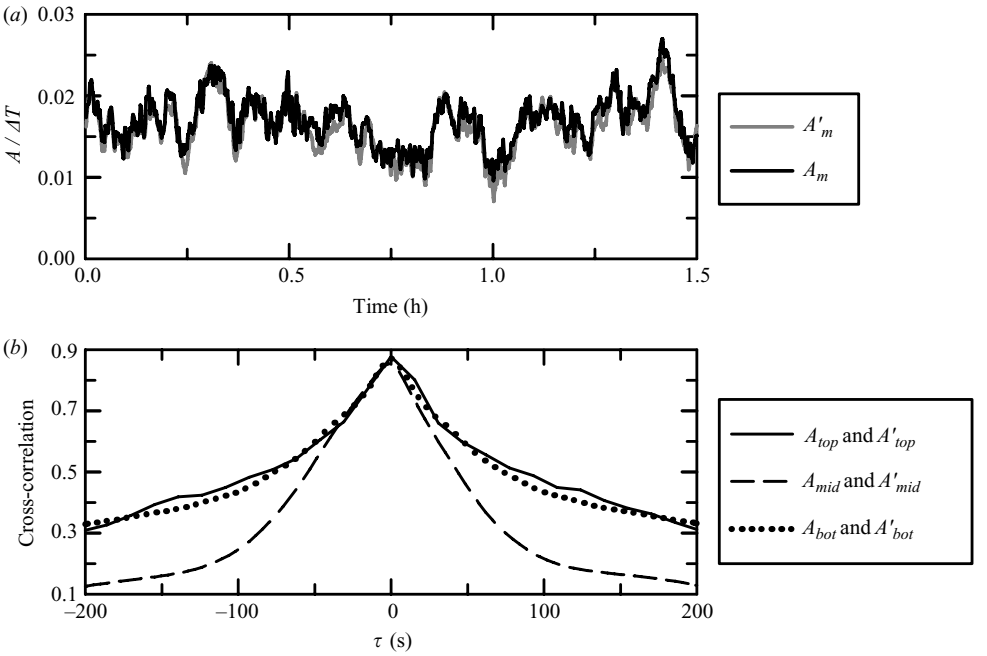

FIGURE 4. (*a*) Time traces of the normalized strength $A_m/\Delta T$ of the LSC obtained using the TEE method and the normalized strength $A'_m/\Delta T$ obtained from the SF method. (*b*) The cross-correlation functions between the strengths obtained using the two different methods for the top (solid line), middle (dashed line) and bottom (dotted line) planes. The data were measured at $Ra = 5.5 \times 10^9$.

Figure 4(*a*) shows the time traces of A_m and A'_m. It is seen that the two time traces are again very similar to each other except that A_m is on average $\sim$5 % larger than A'_m. Figure 4(*b*) shows the cross-correlation functions between A and A' at the three heights. It similarly shows that all three functions have a strong positive correlation with their peaks all located at time lag $\tau = 0$ and the cross-correlation coefficient $C(\tau = 0)$ all being nearly 0.9.

The above results imply that, as far as the orientation and the strength of the LSC are concerned, both the SF and the TEE methods give the same results, but the TEE method in addition determines the LSC's sloshing motion, which is missed by the SF method. This is illustrated in figures 5(*a*) and 5(*b*). It is also clear that the LSC's orientation is determined mainly by the hottest and the coldest azimuthal positions of the bulk fluid along the sidewall. This is not surprising, since one can see from figure 1(*c*) that the sinusoidal fit to the temperature profile shifts the hottest azimuthal position $\alpha_{h,m}$ right or anticlockwise and shifts the coldest azimuthal position $\alpha_{c,m}$ left or clockwise and the changes of the obtained orientation of the LSC due to the two shifts roughly cancel each other.

3. Results and discussion

3.1. *The sloshing oscillation of the LSC at mid-height plane*

The off-centre distance d_m of the LSC's central line at the mid-height plane is used to study the sloshing motion of the LSC at that plane. Figure 6(*a*) shows a typical time trace of the measured d_m normalized by the cell's diameter D. It is seen from the

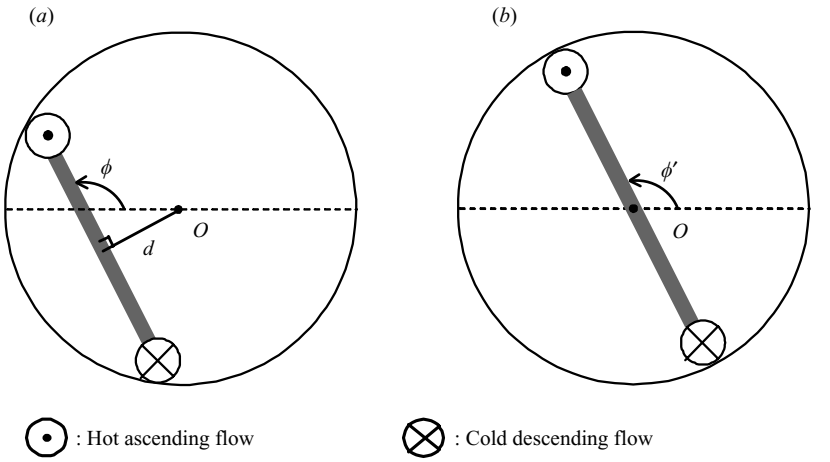

FIGURE 5. (*a*) Schematic diagram showing the definitions of the orientation ϕ and the off-centre distance d of the LSC obtained using the TEE method. (*b*) Schematic diagram showing the definition of the orientation ϕ' of the LSC obtained using the SF method. In this method, the off-centre distance is forced to be always zero.

figure that d_m/D fluctuates around 0. We further found that the temporal averages of d_m/D for all six values of Ra are nearly 0. In Xi *et al.* (2009) a similar trace measured with the in-fluid thermistors in a tilted cell has been shown. For comparison, we plot in figure 6(*b*) a time trace of d_m/D measured under the same conditions as in Xi *et al.* (2009) but with the cell levelled ($0 \pm 0.06^\circ$). It shows that d_m/D measured from the in-fluid probes has a stronger strength and its oscillation looks more periodic when compared with that obtained from the in-wall thermistors. Nevertheless, the physical pictures revealed by the two time traces are the same, i.e. the LSC's central line oscillates horizontally around the cell's central vertical axis. Figure 6(*c*) shows the p.d.f. of d_m/D obtained from the in-wall thermistors (solid circles). The p.d.f. is found to be flatter than a Gaussian function, i.e. the flatness is 2.3. The p.d.f.s obtained at other Ra share the same features as those shown in figure 6(*c*), except for the two lowest Ra. A possible reason for the observed different distributions for small Ra may be the limited resolution of temperature probes. The accuracies of thermistors are determined mainly by the calibration process. For the present study, the 24 in-wall thermistors were calibrated with an accuracy of about 0.01°C. While the amplitude of the azimuthal temperature profile is only ~0.05°C for the lowest Ra in the experiment. The temperature contrast along the sidewall is thus limited and may influence the measured distribution of d_m/D for small Ra. For comparison, we also plot in the same figure the p.d.f. of d_m/D obtained from the in-fluid thermistors (solid circles). It is seen that the in-fluid thermistors reveal a sloshing mode with a larger oscillation range and an approximately equal distribution, which shows that the in-fluid thermistors have a higher sensitivity and are able to measure the sloshing mode more accurately. The difference between the distributions measured from the in-fluid and the in-wall thermistors are due to the sidewall effects as discussed in § 2.1.

As d_m/D oscillates around its mean value of 0, its standard deviation σ_{d_m}/D can be used as a measure of the amplitude of this oscillation. Figure 7(*a*) shows the Ra-dependence of σ_{d_m}/D obtained from the in-wall (solid circles) and in-fluid (open circles) thermistors. One sees that σ_{d_m}/D depends weakly on Ra for the present range of Ra with σ_{d_m}/D from the in-fluid probes being ~60 % larger than that obtained

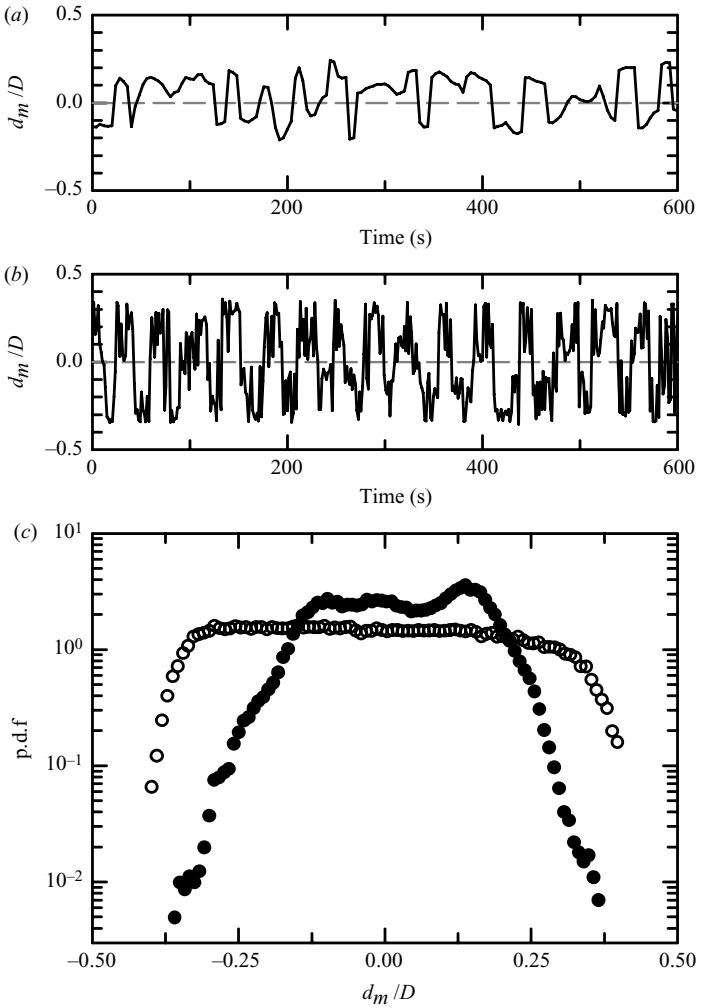

FIGURE 6. Time traces of the normalized off-centre distance d_m/D from thermistors (a) embedded into the sidewall and (b) placed in fluid. (c) p.d.f. of d_m/D from the in-wall (solid circles) and in-fluid (open circles) thermistors. The data of the in-fluid thermistors are taken at $Ra = 5.0 \times 10^9$ with a sampling rate of 0.76 Hz and that of the in-wall probes at $Ra = 5.5 \times 10^9$ with a sampling rate of 0.29 Hz.

from the in-wall thermistors. In Xi *et al.* (2009) it has been shown that the sloshing or off-centre motion of the LSC exhibits a well-defined time-periodic oscillation. The prominent peak near f_0 in the frequency power spectra of d_m (see the second curve from bottom in figure 8a) corresponds to this periodic oscillation. In figure 7(b) we plot the Ra-dependence of the normalized frequency corresponding to this prominent peak obtained from the spectra of d_m. The solid line in the figure represents the power-law fit to the data: $H^2 f_0/\kappa = 0.12 Ra^{0.49\pm0.02}$, with the scaling exponent being in good agreement with the previous temperature measurements in water (Qiu & Tong 2001*a*, 2002; Sun & Xia 2005; Brown, Funfschilling & Ahlers 2007), mercury (Takeshita *et al.* 1996) and low-temperature helium gas (Heslot, Castaing & Libchaber 1987; Castaing *et al.* 1989; Sano, Wu & Libchaber 1989; Niemela *et al.* 2001). This result further indicates that the previously observed temperature oscillations near

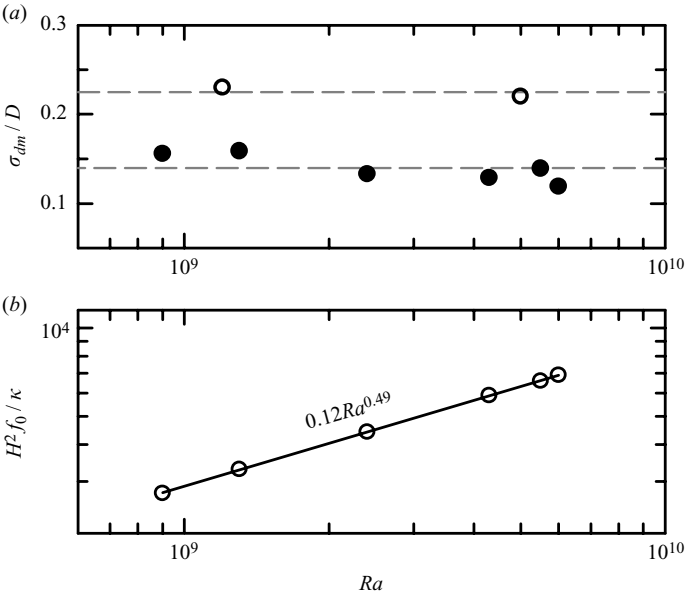

FIGURE 7. (*a*) The *Ra*-dependence of the standard deviation of d_m/D from the in-wall (solid circles) and in-fluid (open circles) thermistors. Two dashed lines show the mean value of σ_{d_m}/D averaged over all *Ra* investigated. (*b*) Normalized oscillation frequency $H^2 f_0/\kappa$ obtained from the frequency power spectra of d_m as a function of *Ra*. The solid line is the power-law fit.

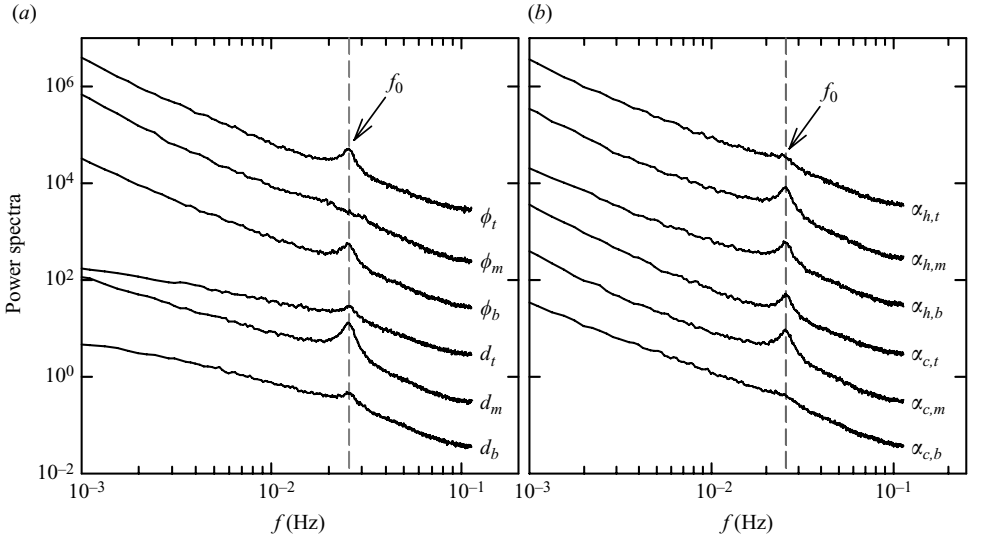

FIGURE 8. Power spectra of (*a*) ϕ_t, ϕ_m, ϕ_b, d_t, d_m, and d_b and (*b*) $\alpha_{h,t}$, $\alpha_{h,m}$, $\alpha_{h,b}$, $\alpha_{c,t}$, $\alpha_{c,m}$, and $\alpha_{c,b}$. All data have been shifted vertically for clarity.

the mid-height of the cell indeed originate from the sloshing oscillation of the LSC. Taken together, the physical picture behind figure 6 is that the LSC's central line oscillates time-periodically around the cell's central vertical axis with an amplitude nearly independent of the turbulent intensity.

3.2. *The relationship between the sloshing and the torsional modes of the LSC*

Figure 8(a) shows, from top to bottom, the frequency power spectra of ϕ_t, ϕ_m, ϕ_b, d_t, d_m and d_b. For the orientations of the LSC obtained at the three heights, the prominent peak near f_0 representing periodic oscillation can be seen clearly for ϕ_t and ϕ_b, but is absent for the mid-height plane (ϕ_m). These are consistent with those observed by Funfschilling *et al.* (2008) and Xi & Xia (2008*b*) and correspond to the twisting mode of the LSC (Funfschilling & Ahlers 2004). Note that the power spectra also show that the sloshing and torsional modes have the same periodicity as determined by the position of the prominent peak. We further found that although ϕ_m will also exhibit oscillation when the cell is tilted by several degrees, the strength of this oscillation obtained at the mid-height plane is much weaker than those of ϕ_t and ϕ_b, i.e. the peak height of the spectra of ϕ_m at f_0 is much smaller than those of ϕ_t and ϕ_b. However, for the off-centre distance, the situation is opposite. In figure 8(a) one sees that the strength of the oscillation peak for d_m at the mid-height plane is much stronger than those of d_t and d_b.

To understand this difference and to find out the relationship between the sloshing mode at the mid-height plane and the torsional mode of the LSC near the top and bottom plates, we examine the frequency power spectra of the azimuthal positions of the hot ascending and cold descending flows at the three heights, as both the orientation ϕ and the off-centre distance d of the LSC are obtained from these positions. Figure 8(b) shows that the spectra of $\alpha_{c,t}$ and $\alpha_{h,b}$ exhibit an oscillation peak near f_0. Whereas the spectra of $\alpha_{h,t}$ and $\alpha_{c,b}$ both give very faint oscillations, which are due to a tilted ellipse-like circulation path of the LSC when viewed from the side (Qiu & Tong 2001*b*; Sun & Xia 2005; Sun *et al.* 2005*b*). The thermistors embedded into the sidewall cannot feel accurately the hot ascending flow of the LSC at the top-plane and the cold descending flow of the LSC at the bottom-plane, since they are far away from the sidewall at the respective heights (figure 1*b*). Therefore, at the top and bottom planes, the in-wall probes may not be able to measure the orientation and the off-centre distance of the LSC as accurately as those at the mid-height plane. This suggests that the relatively weak oscillation peaks of d_t and d_b shown in figure 8(a) are mainly due to the oscillations of $\alpha_{c,t}$ and $\alpha_{h,b}$. The surprising thing shown in figure 8(b) is that the spectra of the azimuthal positions $\alpha_{h,m}$ and $\alpha_{c,m}$ of the hot ascending and cold descending flows at the *mid-height plane* both exhibit a well-defined time-periodic oscillation with the oscillation peak located at f_0 and with the same strength as those of $\alpha_{h,b}$ and $\alpha_{c,t}$. This implies that the azimuthal positions of the hot ascending and cold descending fluids both oscillate periodically along the sidewall irrespective of whether they are near the plates or at the mid-height of the cell.

Figure 9(a) shows typical time traces of $\alpha_{h,b}$ and $\alpha_{h,m}$ measured at the same time. It is seen that the two time traces are rather similar to each other except for a several seconds delay between them. The cross-correlation function $C_{\alpha_{h,m},\alpha_{h,b}}$ shown in figure 9(c) quantifies this similarity. It shows that $\alpha_{h,m}$ and $\alpha_{h,b}$ have a strong positive correlation with the main peak located at $\tau \simeq 6 \pm 1$ s $\simeq (0.21 \pm 0.04)\tau_0$ (Here, $\tau_0 = 1/f_0$ is the oscillation period of the LSC). This positive time-delay indicates that the azimuthal motion of $\alpha_{h,m}$ lags that of $\alpha_{h,b}$, which is easy to understand since the hot ascending flow rises up from bottom. Similar situation can be seen for the relation between $\alpha_{c,t}$ and $\alpha_{c,m}$. Figure 9(b) shows the time traces of $\alpha_{c,t}$ and $\alpha_{c,m}$, which again are quite similar to each other. Figure 9(d) plots $C_{\alpha_{c,m},\alpha_{c,t}}$, and it is found that $\alpha_{c,m}$ correlates strongly with $\alpha_{c,t}$ with a positive time delay $\tau \simeq 5 + 1$ s $\simeq (0.18 \pm 0.04)\tau_0$

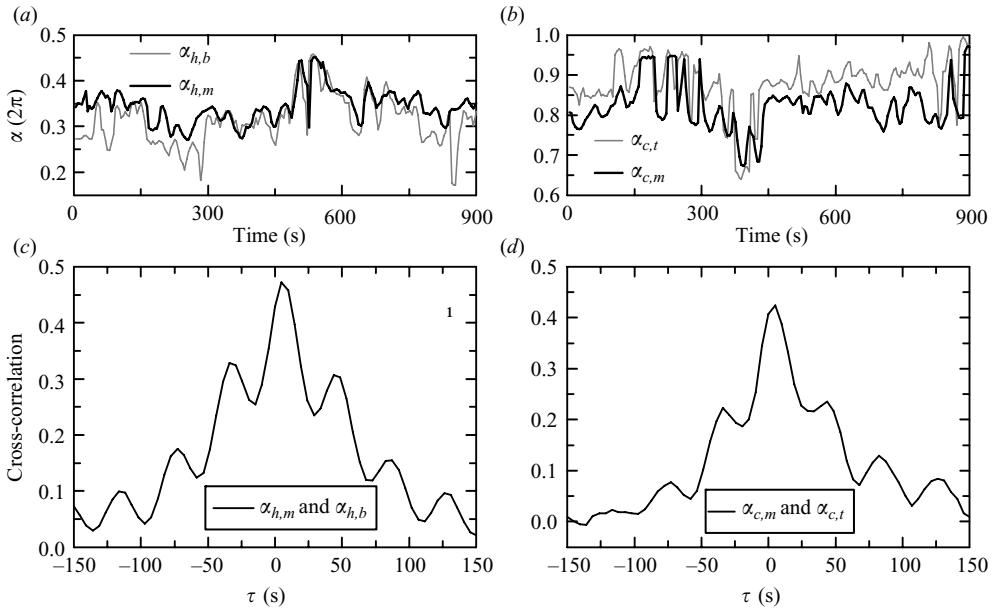

FIGURE 9. Time traces of (*a*) $\alpha_{h,b}$ and $\alpha_{h,m}$ and (*b*) $\alpha_{c,t}$ and $\alpha_{c,m}$. The cross-correlation functions (*c*) between $\alpha_{h,m}$ and $\alpha_{h,b}$ and (*d*) between $\alpha_{c,m}$ and $\alpha_{c,t}$. All data were obtained at $Ra = 5.5 \times 10^9$.

indicating that the azimuthal motion of $\alpha_{c,m}$ lags that of $\alpha_{c,t}$. Here we note that the time delay of the main peak of $C_{\alpha_{c,m},\alpha_{c,t}}$ is essentially the same as that of $C_{\alpha_{h,m},\alpha_{h,b}}$ within experimental uncertainty, this is due to the fact that the distance between the middle and the top planes is the same as the distance between the middle and bottom ones. Note also that the subpeaks of $C_{\alpha_{h,m},\alpha_{h,b}}$ and $C_{\alpha_{c,m},\alpha_{c,t}}$ correspond to the periodic oscillations shown in figure 8(*b*). These results further imply that the hot ascending and cold descending flows go up and fall down coherently, thus propagate their azimuthal positional oscillations along the sidewall.

The torsional mode of the LSC can be revealed by the horizontal motions of the hot ascending and cold descending flows near the top and bottom plates. Here, we define

$$\omega_{i,j} = \frac{\mathrm{d}\alpha_{i,j}}{\mathrm{d}t}, \tag{3.1}$$

as the azimuthal angular velocity of $\alpha_{i,j}$, where $i = h$ or c and $j = t$, m or b. Figure 10(*a*) shows the cross-correlation function $C_{\omega_{c,t},\omega_{h,b}}$ between $\omega_{c,t}$ and $\omega_{h,b}$ (dash-dotted line). It is seen that $C_{\omega_{c,t},\omega_{h,b}}$ oscillates and $\omega_{c,t}$ anticorrelates with $\omega_{h,b}$ with a strong negative peak located at $\tau = 0$. The negative peak at $\tau = 0$ indicates that $\alpha_{c,t}$ rotates clockwise when $\alpha_{h,b}$ rotates anticlockwise and vice versa, implying the twisting motion of the LSC. Recall that the azimuthal motions of $\alpha_{h,m}$ and $\alpha_{c,m}$ follow coherently those of $\alpha_{h,b}$ and $\alpha_{c,t}$, respectively, with the same time delay. The azimuthal angular velocities of $\alpha_{h,m}$ and $\alpha_{c,m}$ would hence be expected to exhibit the same behaviour as those of $\alpha_{h,b}$ and $\alpha_{c,t}$, and this is indeed observed from figure 10(*a*), which shows that $C_{\omega_{c,m},\omega_{h,m}}$ (solid line) is the same as $C_{\omega_{c,t},\omega_{h,b}}$ (dash-dotted line), i.e. periodic oscillations and a strong negative peak at $\tau = 0$. Here, we also plot $C_{\omega_{c,m},\omega_{h,m}}$ obtained from the in-fluid thermistors (dashed line). It is seen that $C_{\omega_{c,m},\omega_{h,m}}$ obtained from the in-fluid thermistors exhibits the oscillation with much stronger periodicity

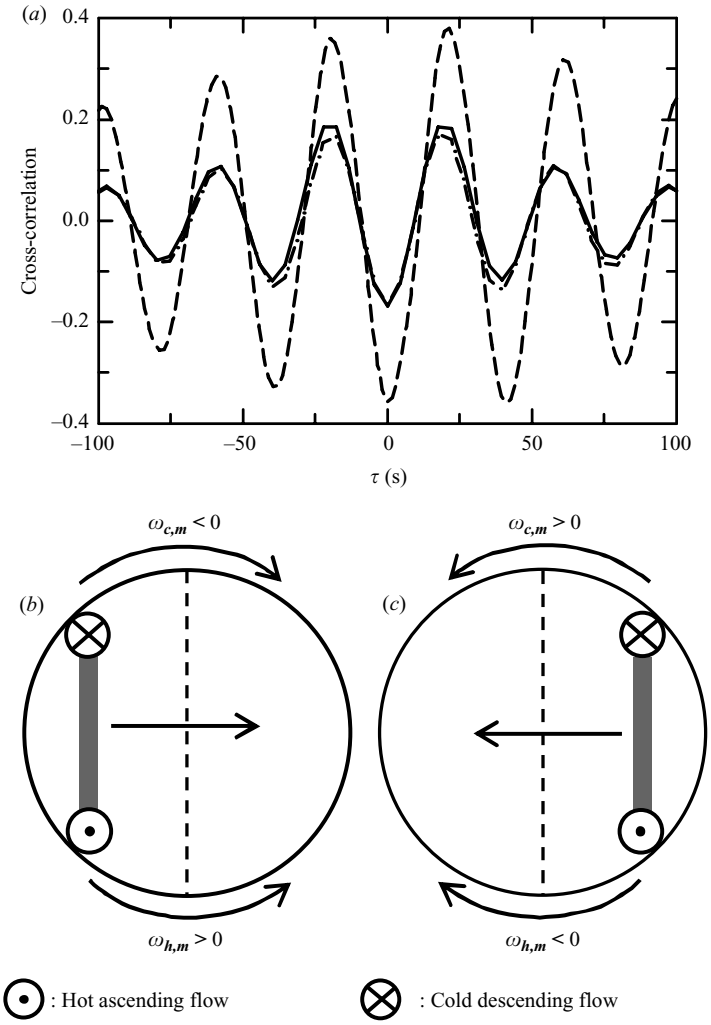

FIGURE 10. (*a*) The cross-correlation functions $C_{\omega_{c,t},\omega_{h,b}}$ (dash-dotted line) and $C_{\omega_{c,m},\omega_{h,m}}$ from the in-wall (solid line) and in-fluid thermistors (dashed line). The data from in-wall thermistors are taken at $Ra = 5.5 \times 10^9$ and those from in-fluid probes at $Ra = 5.0 \times 10^9$. (*b*) Schematic diagram of the azimuthal positions of the hot ascending and cold descending flows when the sloshing oscillation is at an extremum. The curved arrows show the directions of the angular velocities and the horizontal arrow shows the moving direction of the LSC's central line. (*c*) Same as (*b*) but half an oscillation period later.

than that obtained from the in-wall thermistors (solid line). However, the basic picture is the same for both cases. These results indicate that the azimuthal positional oscillations of the hot ascending and cold descending flows at the mid-height plane are out of phase with each other by π, leading to the sloshing mode of the LSC at the mid-height plane. Figures 10(*b*) and 10(*c*) illustrate how the sloshing mode and the torsional mode are connected, as manifested by the horizontal motions of the upward going hot plumes and downward going cold plumes. Figure 10(*b*) shows that $\alpha_{c,m}$ rotates clockwise when $\alpha_{h,m}$ rotates anticlockwise, and the line connecting them thus moves to the right. Half an oscillation period later (figure 10*c*), the motion of $\alpha_{c,m}$ changes to anticlockwise while that of $\alpha_{h,m}$ to clockwise; this makes the LSC

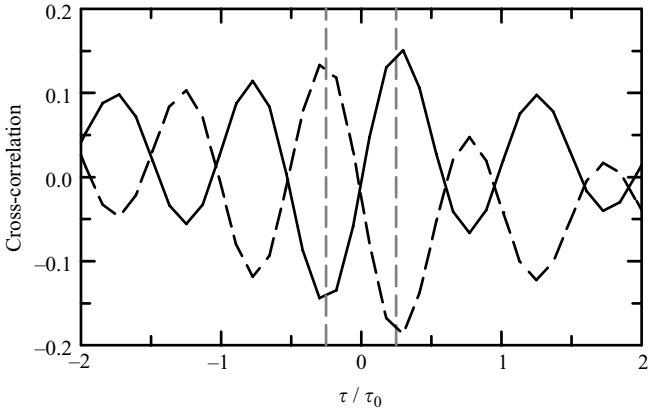

FIGURE 11. The cross-correlation functions $C_{d_m,\phi_b-\phi_m}$ (solid line) and $C_{d_m,\phi_t-\phi_m}$ (dashed line) versus τ/τ_0 obtained at $Ra = 5.5 \times 10^9$. The two vertical dashed lines indicate $\tau = \pm\tau_0/4$. Here $\tau_0 = 1/f_0$ is the oscillation period of the LSC.

central line move to the left. The periodic occurrence of this process thus generates the sloshing oscillation of the LSC and produces the prominent peak near f_0 on the spectra of d_m. On the other hand, as the orientation ϕ_m equals to $(\alpha_{h,m} + \alpha_{c,m})/2$ plus a constant, the anticorrelation between $\omega_{h,m}$ and $\omega_{c,m}$ would cancel out the periodic oscillations, and hence it is not surprising to see in figure 8(*a*) that an oscillation peak is absent for the spectra of ϕ_m.

The phase relationship between the twisting and the sloshing oscillations can be shown more directly by studying their cross-correlation functions. We use the deviations $\phi_t - \phi_m$ and $\phi_b - \phi_m$ of the top and the bottom plane orientations from the orientation of the mid-height plane to characterize the twisting oscillation of the LSC (Funfschilling *et al.* 2008). Figure 11 shows the cross-correlation functions $C_{d_m,\phi_b-\phi_m}$ (solid line) and $C_{d_m,\phi_t-\phi_m}$ (dashed line) versus the normalized delay time τ/τ_0. Here, $\tau_0 = 1/f_0$ is the oscillation period of the LSC. The maximum of $C_{d_m,\phi_b-\phi_m}$ at $\tau \simeq \tau_0/4$ indicates that the twisting oscillation near the bottom plate and the sloshing oscillation at the mid-height plane are out of phase with each other by $\pi/2$ and the sloshing oscillation lags the twisting oscillation near the bottom plate. Similar situation can be seen for the relation between d_m and $\phi_t - \phi_m$, i.e. the maximum of $C_{d_m,\phi_t-\phi_m}$ at $\tau \simeq -\tau_0/4$ indicates that the twisting oscillation near the top plate and the sloshing oscillation at the mid-height plane are also $\pi/2$ out of phase and the sloshing oscillation leads the twisting oscillation near the top plate. Taken together, the twisting oscillation near the top and bottom plates and the sloshing oscillation at the mid-height plane are out of phase with each other by $\pi/2$, i.e. when one is maximally displaced from the mean flow the other is not displaced from the mean flow.

3.3. *Direct velocity measurement of the sloshing motion*

In this subsection we present direct evidence of the sloshing oscillation of the LSC from particle image velocimetry (PIV) measurement of the horizontal velocity field at the mid-height plane in a sapphire cell. Both the sapphire cell and the horizontal velocity measurement using the PIV technique have been described in detail previously (Xi *et al.* 2006; Zhou, Sun & Xia 2007*a*) and hence we outline only their main features here. The sapphire cell consists of two sapphire discs with thickness 5 mm as the top

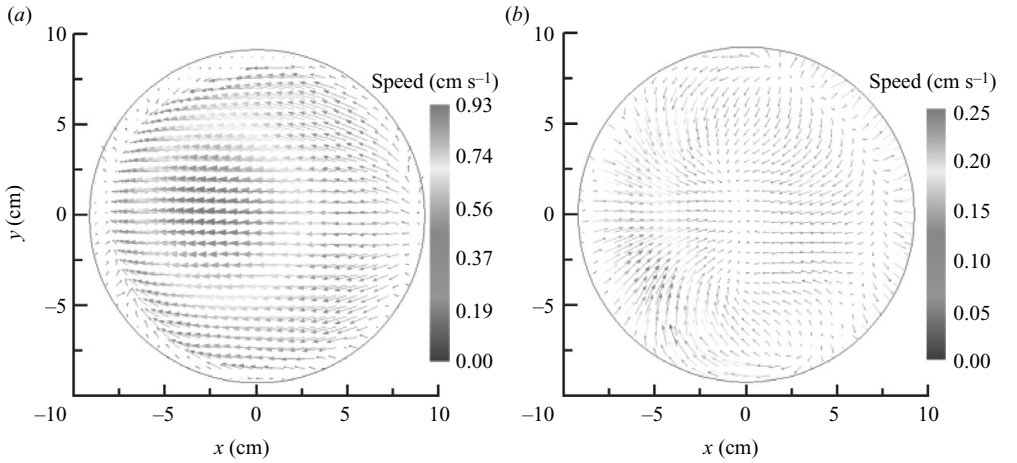

FIGURE 12. Time-averaged velocity vector map measured (*a*) near the top plate and (*b*) at the mid-height plane. For clarity, a coarse-grained vector map of size 32×32 is shown. The magnitude of the velocity $\sqrt{u^2 + v^2}$ is coded in the length of the arrows in cm s^{-1}. Both time averages are taken over a period of 151 min corresponding to 20 000 velocity maps.

and bottom plates and a Plexiglas tube with thickness 8 mm as the sidewall. The cell's inner diameter and height are both 18.5 cm, so the aspect ratio of the cell is also unity. In the present work, 50 μm diameter polyamid spheres (density 1.03 g cm^{-3}) were used as the seeding particles and a horizontal laser light-sheet with thickness ~2 mm was used to illuminate the particles in the mid-height plane of the cell. The measuring area is a square of 18.5×18.5 cm^2, which covers completely the horizontal cross-section of the cell. The spatial resolution is 0.29 cm, corresponding to 63×63 velocity vectors in each two-dimensional velocity map. Denote the laser-illuminated plane as the (x, y)-plane and the centre of the mid-height horizontal cross-section of the cell as the origin O of the coordinates (see figure 14*a*), then two horizontal velocity components $u(x, y)$ and $v(x, y)$ are measured. In these PIV measurements, the cell was tilted by ~1° at position 1, and thus the orientation of the LSC was locked along the x-direction (see figure 1*a*). For the PIV experiment, the measurements were made at $Ra = 3.0 \times 10^9$ and 6.0×10^9 and at $Pr = 4.3$. A total of 20 000 vector maps were acquired for each Ra at a sampling rate of ~2.2 Hz. As the two measurements give the same results, results only for $Ra = 6.0 \times 10^9$ will be presented.

To study the global motion of the central bulk fluid, we use the velocity vector $\boldsymbol{V}(t) = V_x(t)\hat{\boldsymbol{x}} + V_y(t)\hat{\boldsymbol{y}}$ to characterize the overall flow behaviour at the mid-height plane, where $V_x(t)$ and $V_y(t)$ are the spatial averages of the local velocity components $u(t)$ and $v(t)$, respectively, within a circular area centred at the centre of the measurement area. The diameter of the circular area is 5 cm and there are 221 vectors contained in this circular region for averaging. A circle with a diameter of 10 cm has also been used and the obtained results are essentially the same (see Xi *et al.* 2006). The orientation $\theta \equiv \arctan(V_y/V_x)$ and the magnitude $V \equiv |\boldsymbol{V}| = \sqrt{V_x^2 + V_y^2}$ of the averaged vector are then measures of the orientation and the strength of the motion of the central bulk fluid, respectively.

Note that the horizontal velocity field investigated in Xi *et al.* (2006) was obtained near the top plate. Figure 12(*a*) shows the time-averaged velocity vector map measured at 2 cm from the top plate, where the LSC is dominated mainly by the horizontal velocities. Therefore, the spatially averaged velocity vector $\boldsymbol{V}(t)$ measured at the

horizontal planes near the top plate can be used as a measure of the orientation vector $\boldsymbol{V}_{LSC}$ of the LSC and its orientation θ can be used to characterize the orientation of the LSC at the corresponding height. Indeed, Xi *et al.* (2006) have used the properties of $\boldsymbol{V}$ and θ measured near the top plate to characterize the azimuthal motion of the LSC in turbulent RB system. However, the situation is different when the measurement is made near the cell's mid-height plane, which is the case here. This is because at the cell's mid-height plane the LSC is concentrated near the sidewall and dominated mainly by vertical velocities, as shown in figure 12(*b*) (see also the circulation path of the LCS in figure 1(*b*)). Thus, the velocity vector $\boldsymbol{V}(t)$ spatially averaged from the velocities measured near cell centre cannot be used to represent the orientation vector of the LSC and its orientation θ is no longer a direct measure of the LSC's orientation. Therefore, θ measured at the mid-height plane and ϕ_m (the orientation of the LSC obtained from the azimuthal temperature profile) would exhibit different behaviours. As we shall see below, this is indeed the case.

Figure 13(*a*) shows the p.d.f. of the measured velocity orientation θ. It is seen that the p.d.f. of θ, which is significantly different from that of ϕ_m in figure 3(*c*), exhibits a bimodal distribution with two peaks located at the orientations ($\theta = \pm 0.25$) that are perpendicular to the preferred orientation of the LSC ($\theta = 0$). The probabilities of $\theta = \pm 0.25$ are nearly three times larger than those of $\theta = 0$ and $\theta = \pm 0.5$, suggesting that the central bulk fluid is much more likely to move in the direction perpendicular to the LSC's vertical circulation plane rather than in the LSC's preferred direction itself. To study the flow strength of the central bulk fluid in different orientations, we calculate the conditional average $\langle V|\theta \rangle$ on the velocity orientation θ, as shown in figure 13(*b*). One sees that the averaged-velocity magnitudes in the directions ($\theta = \pm 0.25$) perpendicular to the LSC plane are much stronger than the magnitudes in all other directions, especially than those in the preferred direction of the LSC. Figure 13(*c*) shows the auto-correlation functions C_{V_x} (dashed line) and C_{V_y} (solid line). Both show oscillations, but the oscillation strength of V_y (in the direction perpendicular to the LSC plane) is much stronger than that of V_x (along the LSC's preferred direction) and V_y oscillates more coherently than V_x. In fact, a previous single-point velocity measurement has shown that at the cell centre the strongest velocity oscillation is along the direction perpendicular to the LSC plane and that the strength of this oscillation decays away from the cell centre towards the plates (Qiu *et al.* 2004; Sun *et al.* 2005*b*). We further note that the oscillation frequency of V_y is the same as that of the sloshing motion of the LSC but 20 % larger than that of V_x. Different oscillation frequencies for V_x and V_y have also been observed, but not explicitly recognized, by Qiu *et al.* (2004) and Sun *et al.* (2005*b*). The existence of two different oscillation frequencies in turbulent convection with fixed control parameters (Ra and Pr) have already been observed previously. Xi *et al.* (2006) studied the azimuthal motion of the LSC near the top plate and they found that although the magnitude and the orientation of the LSC both exhibit oscillations, the oscillation of the LSC's magnitude is slower than that of the LSC's orientation. Brown *et al.* (2007) compared the twisting-oscillation period of the LSC (or the oscillation of the LSC's orientation) and the plume turnover time (determined from the auto-correlation and cross-correlation of temperature in their case) and their results showed that above a critical Rayleigh number (e.g. 3×10^9 for $Pr = 4.3$) the twisting-oscillation period of the LSC is longer than the plume turnover time. Taking all these results together, it seems that there exist at least three different oscillation frequencies in turbulent RB system. Xia (2007) suggested that different oscillation frequencies may indicate the presence of more than one clocks (or more than one driving mechanism) in turbulent

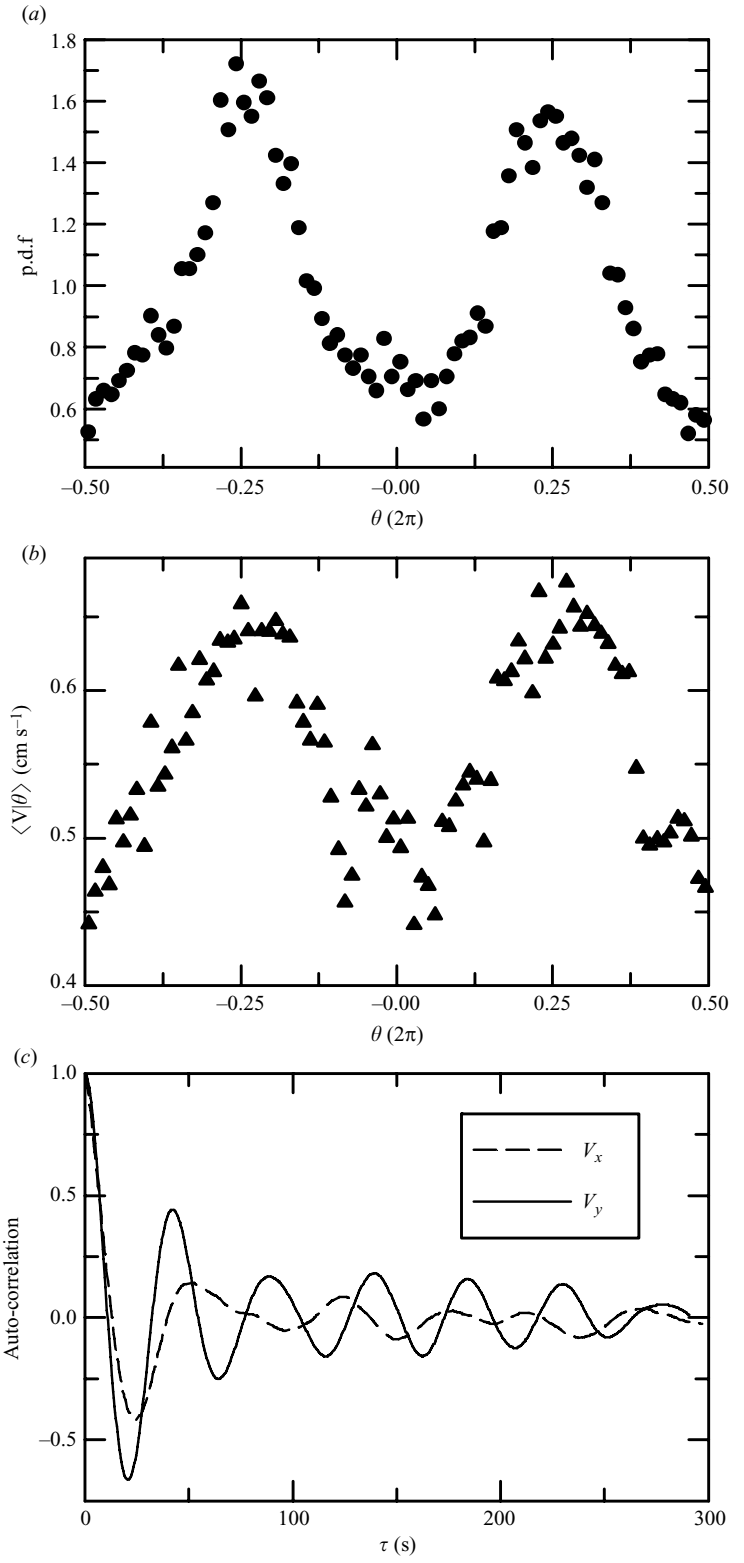

FIGURE 13. (*a*) p.d.f. of the orientation θ of the spatially averaged vector $\boldsymbol{V}$. (*b*) The conditional average $\langle V|\theta\rangle$ on the velocity orientation θ. (*c*) The auto-correlation functions of V_x and V_y.

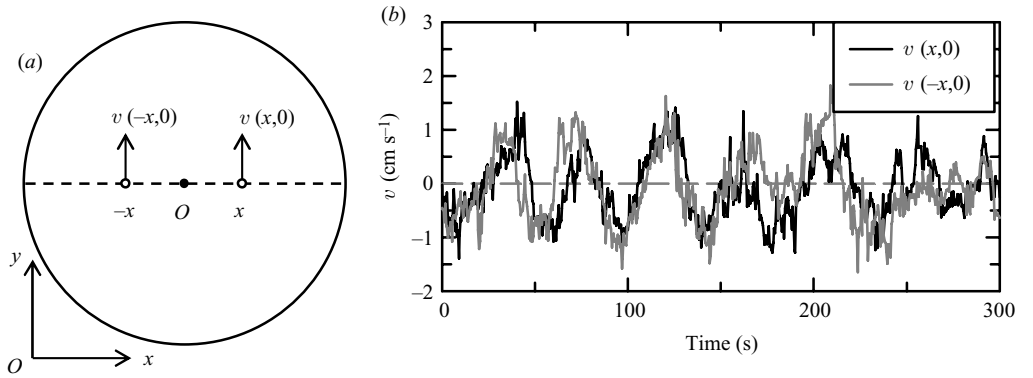

FIGURE 14. (*a*) Coordinate system and schematic diagram of the mid-height horizontal cross-section of the cell. The origin O of the coordinates is chosen as the centre of the cross-section and thus the z-axis (not shown in the figure) is along the cell's central vertical axis. The two vertical arrows show the velocity components v located at positions $(x, 0)$ and $(-x, 0)$ and the dashed line shows the x-axis. (*b*) Time traces of $v(x, 0)$ and $v(-x, 0)$ for $x/D = 0.11$.

RB system, but pointed out that this requires further experimental verifications. An alternative explanation is that there exists only one driving mechanism or clock in the system and that the oscillations in the different quantities are driven by the same clock. Because of the presence of a strongly turbulent background, this oscillation is damped to a varying degree or by different mechanisms in the various quantities, resulting in the difference in the measured frequencies of these quantities. Notwithstanding the above, the overall picture emerging from the PIV measurements is that the translational motion of the central bulk fluid in the direction perpendicular to the LSC's vertical circulation plane is more probable, much stronger and more coherent than the motions in all other directions, which provides a direct evidence for the sloshing motion of the LSC at the mid-height plane.

In a previous work, Sun *et al.* (2005*b*) measured the two-dimensional velocity field in the (y, z)-plane, which is perpendicular to the LSC's vertical circulation plane and studied the phase relationships among the horizontal velocity components $v(y)$ along the y-axis and among $v(z)$ along the z-axis. For $v(y)$ along the y-axis, their results showed that the velocity component $v(y)$ at different values of y are highly correlated and have a common phase across the cell's entire diameter. For $v(z)$ along the z-axis, their results revealed that the horizontal velocity component $v(z)$ at different height z remains in phase along the z-axis mainly in the middle one-half of the cell, while the horizontal velocity components $v(z)$ near the upper and lower conducting plates gradually lag behind those in the central region of the cell. Both of these results imply that the motion of the central bulk fluid is spatially coherent and the sloshing oscillation is the dominant mode of the central bulk fluid motion.

The bulk sloshing mode of the flow field can also be revealed by investigating the variation along the x-axis of the y-velocity component $v(x, 0)$. Here we study the relationship between $v(x, 0)$ and $v(-x, 0)$ for various values of $x(>0)$. If the azimuthal rotation is the dominant motion of the LSC, $v(x, 0)$ should anticorrelate with $v(-x, 0)$, i.e. $v(x, 0)$ is along the y-direction when $v(-x, 0)$ is along the $-y$-direction and vice versa. While $v(x, 0)$ correlates strongly with $v(-x, 0)$ for the situation that the sloshing motion is the LSC's dominant mode, i.e. $v(x, 0)$ and $v(-x, 0)$ are along the same direction. Figure 14(*b*) shows the typical time series

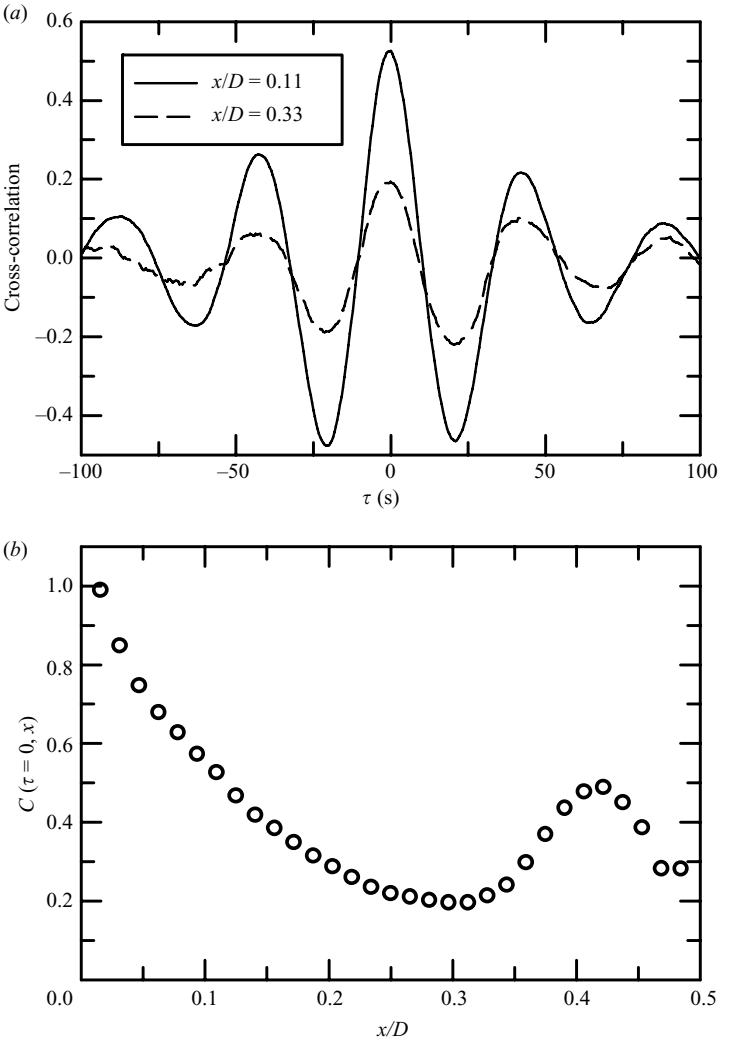

FIGURE 15. (*a*) The cross-correlation functions $C(\tau, x)$ between $v(x, 0)$ and $v(-x, 0)$ for $x/D = 0.11$ (solid line) and 0.33 (dashed line). (*b*) The cross-correlation coefficient $C(\tau = 0, x)$ as a function of x.

of $v(x, 0)$ and $v(-x, 0)$ for $x/D = 0.11$. It is seen that $v(x, 0)$ and $v(-x, 0)$ are very similar to each other and along the same direction for most of the time. In addition, both $v(x, 0)$ and $v(-x, 0)$ are found to exhibit a well-defined periodic oscillation, corresponding to the sloshing oscillation of the LSC. To characterize quantitatively these features, figure 15(*a*) shows the cross-correlation functions $C(\tau, x)$ between $v(x, 0)$ and $v(-x, 0)$ for $x/D = 0.11$ (solid line) and 0.33 (dashed line). It shows that both functions oscillate and have a large positive peak located at $\tau = 0$, indicating that $v(x, 0)$ correlates strongly with $v(-x, 0)$. It is further found that this peak exists for all x and all horizontal velocity oscillations of $v(x, 0)$ have a common phase across the cell's entire diameter. Figure 15(*b*) shows the cross-correlation coefficient $C(\tau = 0, x)$ as a function of x. One sees that $C(\tau = 0, x) \gtrsim 0.2$ for all x and it has a peak near the sidewall (around $x/D \simeq 0.42$). The peak of $C(\tau = 0, x)$ near the sidewall

represents the anticorrelation between $\omega_{h,m}$ and $\omega_{c,m}$, i.e. the sloshing motion of the LSC, as illustrated in figures 10(*b*) and 10(*c*). Both the strong positive peak located at $\tau = 0$ and the oscillation of the cross-correlation functions $C(\tau, x)$ between $v(x, 0)$ and $v(x, 0)$ for all x reveal the fact that the dominant motion of the LSC at the mid-height plane is indeed the sloshing oscillation, which provides another direct evidence for the sloshing mode of the LSC at the mid-height plane.

4. Conclusion

To conclude, we have made a detailed experimental study of the oscillations of the LSC in a cylindrical turbulent RB convection cell with aspect ratio unity using water as working fluid. Direct spatial measurements of both the temperature and velocity fields were carried out to study the motion of the LSC.

Direct measurements of the horizontal velocity field at the cell's mid-height plane using the PIV technique were made at $Ra = 3.0 \times 10^9$ and 6.0×10^9 and $Pr = 4.3$. It is found that the horizontal translational motion of the central bulk fluid in the direction perpendicular to the vertical circulation plane of the LSC is more probable, much stronger and more coherent than the motions in all other directions. For the velocity component $v(x, 0)$ perpendicular to the LSC plane, $v(x, 0)$ for all values of x are found to correlate strongly with each other, especially for the velocities near the sidewall, and have a common phase across the cell's entire diameter. Both of these results provide direct evidences for the sloshing mode of the bulk flow dynamics near the mid-height plane.

The temperature measurement was performed over the Rayleigh number range $9 \times 10^8 \leqslant Ra \leqslant 6 \times 10^9$ and at fixed Prandtl number $Pr = 5.3$. At each Ra the instantaneous azimuthal temperature profile along the sidewall at three different heights, i.e. $H/4$, $H/2$ and $3H/4$ from the bottom plate, was measured. To study the motion of the LSC, we developed a new method, the TEE method. Using this method, the azimuthal angular positions of the hot ascending and cold descending flows at each height were obtained by making a quadratic fit around the highest and the lowest temperature readings, respectively, and the line connecting these two positions is the central line of the LSC band (when viewed from the top). The orientation of this line is thus the orientation of the LSC and the distance between this line and the cell's central vertical axis is defined as the off-centre distance. The motion of the LSC is therefore decomposed into two different modes: the azimuthal mode and the translational or sloshing mode. When compared to the SF method, it is found that, as far as the azimuthal motion of the LSC is concerned, the two methods give the same information in terms of both the orientation and the flow strength of the LSC, while the TEE method can in addition determine the LSC's sloshing motion that is missed by the SF method. With the TEE method, the LSC's central line is found to oscillate time-periodically around the cell's central vertical axis with an amplitude being nearly independent of the turbulent intensity, leading to the sloshing mode of the LSC.

It is well known that in turbulent RB convection the LSC is self-organized from thermal plumes (Xi *et al.* 2004) and it is driven by the buoyancy of the plumes (Xia *et al.* 2003). We have now shown that the horizontal motions of the plumes are in turn modulated by the velocity field itself. Thus, as far as the horizontal motion of the flow is concerned, the plumes behave as passive tracers. This allows us to determine the motion of the LSC from the azimuthal positions of the hottest and the coldest fluids, based on the temperature measurement. This also suggests that the out-of-phase azimuthal positional oscillations of the hot ascending and cold

descending flows are manifestations of the torsional and sloshing modes of the LSC. When these two flows are near the top and bottom plates, the observed motion of the LSC is torsional. When they are near the mid-height plane, the observed motion of the LSC is the sloshing oscillation. It should be stressed that this positional oscillation of the hot and cold fluids does not imply periodic emission of plumes from the plates. In fact, in a recent experimental work, Xi *et al.* (2009) have shown that the temperatures in the thermal boundary layers in regions where plumes are emitted show no oscillations but the temperatures measured just outside the thermal boundary layer show strong oscillations, i.e. only *after* plumes left from the boundary layers do they exhibit oscillatory behaviour. This is also evidenced by our PIV measurements. Our results show that the bulk fluids in the cell's central region exhibit a strong and coherent oscillation across the cell diameter in the direction perpendicular to the LSC. This cannot be caused by the horizontal oscillations of the hot ascending and cold descending plumes near the sidewall (since the fluid is not rigid body), rather, the plume motions are just manifestations of the velocity field oscillation. This further shows that, as far as horizontal motion is concerned, the plumes are being driven by, instead of driving, the bulk flow. Therefore, the horizontal positional oscillations of the hottest and the coldest fluids are due to the modulation of the bulk flow dynamics rather than originating from the boundary layer.

Further investigations about the phase relation between the torsional and the sloshing modes showed that there is a $\pi/2$ phase difference between the two modes. This constant phase difference, together with their same oscillation frequency, suggests that the two modes have the same origin. Perhaps a related oscillation phenomenon in a different type of flow system, where a recirculation that couples boundary layers induces the oscillation that also displays an azimuthal precession, has been studied and explained by the boundary layer coupling model (Rehab, Villermaux & Hopfinger 1997). However, the detailed mechanism for the oscillation dynamics in the turbulent RB convection remains unknown, which will be the focus of future studies.

We gratefully acknowledge support of this work by the Hong Kong Research Grants Council under Grant Nos. CUHK 403806, 403807 and 404307.

REFERENCES

Ahlers, G., Grossmann, S. & Lohse, D. In press Heat transfer and large scale dynamics in turbulent Rayleigh–Bénard convection. *Rev. Mod. Phys.*

Ashkenazi, S. & Steinberg, V. 1999 High Rayleigh number turbulent convection in a gas near the gas–liquid critical point. *Phys. Rev. Lett.* **83**, 3641–3644.

Brown, E. & Ahlers, G. 2006 Rotations and cessations of the large-scale circulation in turbulent Rayleigh–Bénard convection. *J. Fluid Mech.* **568**, 351–386.

Brown, E., Funfschilling, D. & Ahlers, G. 2007 Anomalous Reynolds-number scaling in turbulent Rayleigh–Bénard convection. *J. Stat. Mech.* P10005.

Brown, E., Nikolaenko, A. & Ahlers, G. 2005 Reorientation of the large-scale circulation in turbulent Rayleigh–Bénard convection. *Phys. Rev. Lett.* **95**, 084503.

Burr, U., Kinzelbach, W. & Tsinober, A. 2003 Is the turbulent wind in convective flows driven by fluctuations? *Phys. Fluids* **15**, 2313–2320.

Castaing, B., Gunaratne, G., Heslot, F., Kadanoff, L., Libchaber, A., Thomae, S., Wu, X.-Z., Zaleski, S. & Zanetti, G. 1989 Scaling of hard thermal turbulence in Rayleigh–Bénard convection. *J. Fluid Mech.* **204**, 1–30.

Ciliberto, S., Cioni, S. & Laroche, C. 1996 Large-scale flow properties of turbulent thermal convection. *Phys. Rev.* E **54**, R5901–R5904.

Cioni, S., Ciliberto, S. & Sommeria, J. 1997 Strongly turbulent Rayleign–Bénard convection in mercury: comparison with results at moderate Prandtl number. *J. Fluid Mech.* **335**, 111–140.

Funfschilling, D. & Ahlers, G. 2004 Plume motion and large-scale circulation in a cylindrical Rayleigh-Benard cell. *Phys. Rev. Lett.* **92**, 194502.

Funfschilling, D., Brown, E. & Ahlers, G. 2008 Torsional oscillations of the large-scale circulation in turbulent Rayleigh–Bénard convection. *J. Fluid Mech.* **607**, 119–139.

Heslot, F., Castaing, B. & Libchaber, A. 1987 Transitions to turbulence in helium gas. *Phys. Rev.* A **36**, 5870–5873.

Krishnamurti, R. & Howard, L. N. 1981 Large-scale flow generation in turbulent convection. *Proc. Natl. Acad. Sci. USA* **78**, 1981–1985.

Lam, S., Shang, X.-D., Zhou, S.-Q. & Xia, K.-Q. 2002 Prandtl number dependence of the viscous boundary layer and the Reynolds numbers in Rayleigh–Bénard convection. *Phys. Rev.* E **65**, 066306.

Mashiko, T., Tsuji, Y., Mizuno, T. & Sano, M. 2004 Instantaneous measurement of velocity fields in developed thermal turbulence in mercury. *Phys. Rev.* E **69**, 036306.

Niemela, J. J., Skrbek, L., Sreenivasan, K. R. & Donnelly, R. J. 2001 The wind in confined thermal convection. *J. Fluid Mech.* **449**, 169–178.

Niemela, J. J. & Sreenivasan, K. R. 2006 Turbulent convection at high Rayleigh numbers and aspect ratio 4. *J. Fluid Mech.* **557**, 411–422.

du Puits, R., Resagk, C. & Thess, A. 2007 Breakdown of wind in turbulent thermal convection. *Phys. Rev.* E **75**, 016302.

Qiu, X.-L., Shang, X.-D., Tong, P. & Xia, K.-Q. 2004 Velocity oscillations in turbulent Rayleigh–Bénard convection. *Phys. Fluid* **16**, 412–423.

Qiu, X.-L. & Tong, P. 2001*a* Onset of coherent oscillations in turbulent Rayleigh–Bénard convection. *Phys. Rev. Lett.* **87**, 094501.

Qiu, X.-L. & Tong, P. 2001*b* Large-scale velocity structures in turbulent thermal convection. *Phys. Rev.* E **64**, 036304.

Qiu, X.-L. & Tong, P. 2002 Temperature oscillations in turbulent Rayleigh–Bénard convection. *Phys. Rev.* E **66**, 026308.

Qiu, X.-L., Yao, Y.-S. & Tong, P. 2000 Large-scale coherent rotation and oscillation in turbulent thermal convection. *Phys. Rev.* E **61**, R6075–6078.

Rehab, H., Villermaux, E. & Hopfinger, E. J. 1997 Flow regimes of large-velocity-ratio coaxial jets. *J. Fluid Mech.* **345**, 357–381.

Resagk, C., du Puits, R., Thess, A., Dolzhansky, F. V., Grossmann, S., Fontenele Araujo, F. & Lohse, D. 2006 Oscillations of the large scale wind in turbulent thermal convection. *Phys. Fluids* **18**, 095105.

Sano, M., Wu, X.-Z. & Libchaber, A. 1989 Turbulence in helium-gas free convection. *Phys. Rev.* A **40**, 6421–6430.

Shang, X.-D. & Xia, K.-Q. 2001 Scaling of the velocity power spectra in turbulent thermal convection. *Phys. Rev.* E **64**, 065301 (R).

Siggia, E. D. 1994 High Rayleigh number convection. *Annu. Rev. Fluid. Mech.* **26**, 137–168.

Sreenivasan, K. R., Bershadskii, A. & Niemela, J. J. 2002 Mean wind and its reversal in thermal convection. *Phys. Rev.* E **65**, 056306.

Sun, C., Xi, H.-D. & Xia, K.-Q. 2005*a* Azimuthal symmetry, flow dynamics, and heat transport in turbulent thermal convection in a cylinder with an aspect ratio of 0.5. *Phys. Rev. Lett.* **95**, 074502.

Sun, C. & Xia, K.-Q. 2005 Scaling of the Reynolds number in turbulent thermal convection. *Phys. Rev.* E **72**, 067302.

Sun, C. & Xia, K.-Q. 2007 Multi-point local temperature measurements inside the conducting plates in turbulent thermal convection. *J. Fluid Mech.* **570**, 479–489.

Sun, C., Xia, K.-Q. & Tong, P. 2005*b* Three-dimensional flow structures and dynamics of turbulent thermal convection in a cylindrical cell. *Phys. Rev.* E **72**, 026302.

Takeshita, T., Segawa, T., Glazier, J. A. & Sano, M. 1996 Thermal turbulence in mercury. *Phys. Rev.* E **76**, 1465–1468.

Tilgner, A., Belmonte, A. & Libchaber, A. 1993 Temperature and velocity profiles of turbulent convection in water. *Phys. Rev.* E **47**, R2253–R2256.

Tsuji, Y., Mizuno, T., Mashiko, T. & Sano, M. 2005 Mean wind in convective turbulence of mercury. *Phys. Rev. Lett.* **94**, 034501.

Villermaux, E. 1995 Memory-induced low frequency oscillations in closed convection boxes. *Phys. Rev. Lett.* **75**, 4618–4621.

Xi, H.-D., Lam, S. & Xia, K.-Q. 2004 From laminar plumes to organized flows: the onset of large-scale circulation in turbulent thermal convection. *J. Fluid Mech.* **503**, 47–56.

Xi, H.-D. & Xia, K.-Q. 2007 Cessations and reversals of the large-scale circulation in turbulent thermal convection. *Phys. Rev.* E **75**, 066307.

Xi, H.-D. & Xia, K.-Q. 2008*a* Flow mode transitions in turbulent thermal convection. *Phys. Fluids* **20**, 055104.

Xi, H.-D. & Xia, K.-Q. 2008*b* Azimuthal motion, reorientation, cessation, and reversal of the large-scale circulation in turbulent thermal convection: a comparative study in aspect ratio one and one-half geometries. *Phys. Rev.* E **78**, 036326.

Xi, H.-D., Zhou, Q. & Xia, K.-Q. 2006 Azimuthal motion of the mean wind in turbulent thermal convection. *Phys. Rev.* E **73**, 056312.

Xi, H.-D., Zhou, S.-Q., Zhou, Q., Chan, T.-S. & Xia, K.-Q. 2009 Origin of the temperature oscillation in turbulent thermal convection. *Phys. Rev. Lett.* **102**, 044503.

Xia, K.-Q. 2007 Two clocks for a single engine in turbulent convection. *J. Stat. Mech.* N11001.

Xia, K.-Q., Sun, C. & Zhou, S.-Q. 2003 Particle image velocimetry measurement of the velocity field in turbulent thermal convection. *Phys. Rev.* E **68** 066303.

Zhou, Q., Sun, C. & Xia, K.-Q. 2007*a* Morphological evolution of thermal plumes in turbulent Rayleigh–Bénard convection. *Phys. Rev. Lett.* **98**, 074501.

Zhou, S.-Q., Sun, C. & Xia, K.-Q. 2007*b* Measured oscillations of the velocity and temperature fields in turbulent Rayleigh–Bénard convection in a rectangular cell. *Phys. Rev.* E **76**, 036301.